LAL 87-07
Jan. 1987

Laboratoire de l'Accélérateur Linéaire

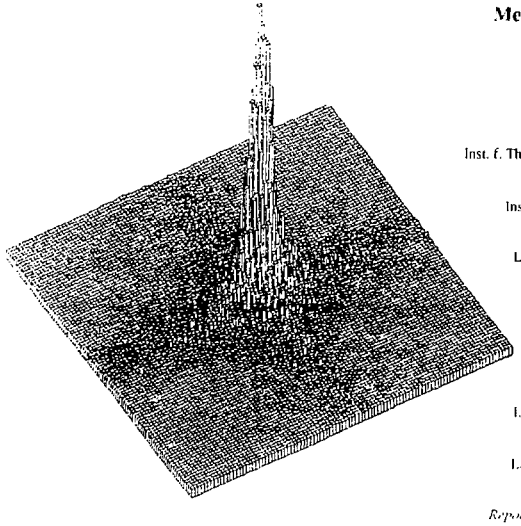

Measurement of the W mass at LEP 200

I. BUNENS and D. ZEPPENFELD
DESY, Hambourg, Germany

Z. KUNSZT, M. POHL and D. WYLER
Inst. f. Theoretical Physik, E.T.H., Hönggerberg, Zürich, Switzerland

P. MINKOWSKI
Inst. f. Theor. Physik, University of Bern, Switzerland

J. BADIER
L.P.N.H.E., Ecole Polytechnique, Palaiseau, France

A.N. DIDDENS and J. TIMMERMANS
NIKHEF-H, Amsterdam, Netherlands

J. LUDWIG and T. POSER
Fakultät für Physik, Freiburg, Germany

H.U. MARTYN
I. Physikalisches Institut, RWTH Aachen, Germany

P. ROUDEAU
Laboratoire de l'Accélérateur Linéaire, Orsay, France

Report from the Working Group on W Mass Measurement.
Presented at the ECFA LEP 200 WORKSHOP
Aachen, Germany, Sept. 29-Oct. 1, 1986

U.E.R
de
l'Universite Paris-Sud

Institut National
de Physique Nucleaire
et
de Physique des Particules

Bâtiment 200 - 91405 ORSAY Cedex

LAL 87-07
Jan. 1987

MEASUREMENT OF THE W MASS AT LEP 200

J. Bijnens and D. Zeppenfeld
Desy, Hamburg, Germany

Z. Kunszt, M. Pohl and D. Wyler
Institut fur Theoretical Physik, E.T.H. Honggerberg, Zurich, Switzerland

P. Minkowski
Institut fur Theoretical Physik, University of Bern, Switzerland

J. Bagler
L.P.N.H.E., Ecole Polytechnique, Palaiseau, France.

A.N. Diddens and J. Timmermans
NIKHEF-H, Amsterdam, Netherlands.

J. Ludwig and T. Poser
Fakultät fur Physik, Freiburg, Germany

H.U. Martyn
I. Physikalisches Institut, RWTH Aachen, Germany

P. Roudeau
Laboratoire de l'Accélérateur Linéaire, Orsay, France

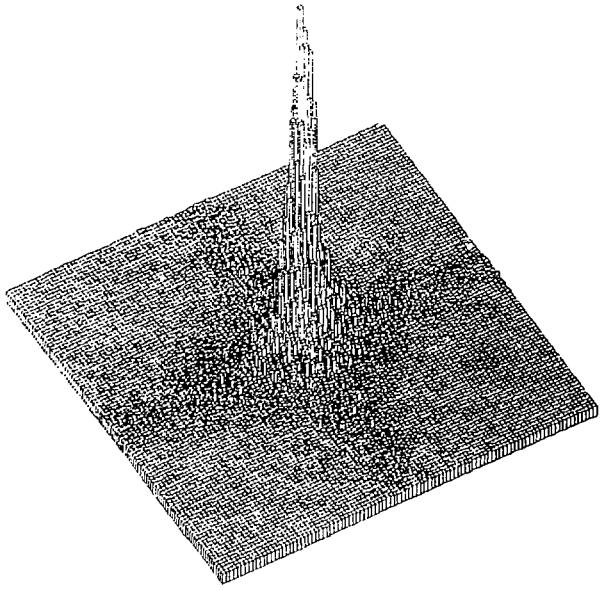

1. INTRODUCTION

During the coming years, the mass of the Z^0 particle and the value of $\sin^2\theta_W$ will be accurately measured at LEP I and SLC. For the first time, these measurements will be sensitive to the electroweak radiative corrections and any deviation from the values expected in the framework of the Standard Model can be interpreted in terms of the existence of heavy quarks, Higgs particles, other generations, ... But, to prove the real manifestation of the Standard Model there is a need for an other measurement at least with the same level of accuracy. We believe that the only place where this can be achieved in the foreseeable future is LEP 200. All the accurate methods we propose use the knowledge of the machine beam energy which has to be precisely measured and stable[1].

2. W PRODUCTION AT e^+e^- MACHINES

In an electron collider, with a beam energy of about 100 GeV, several mechanisms can contribute to the production of W and Z particles. The corresponding cross sections and the decay angular distributions of the produced particles can be accurately computed in the framework of the Standard Model.

2.1 W production in γ-γ collisions

Such a process has a very small cross section ($\sim 10^{-2}$ pb) and can be neglected in this energy domain.

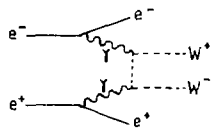

2.2 Single W or Z production[2]

2.2.1 Z production

Radiative corrections to the e^+e^- annihilation cross section into hadrons are the source of the process $e^+e^- \rightarrow \gamma Z^0 (\gamma)$. We note (γ) any additional photon produced in these events. This cross section is large and in practice, the "visible" cross-section depends on the acceptance cuts imposed on the high energy "monochromatic" photon. For instance $\sigma \sim 16$pb for $\theta_\gamma > 10°$ and $E_\gamma > 50$ GeV ($m_\gamma > M_{Z^0}/2$) at $E_b = 95$ GeV.

In addition to this mechanism, photons radiated by one incoming beam particle can produce a Z^0 when they interact with the other beam particle.

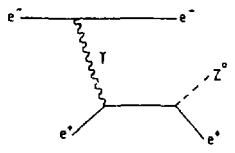

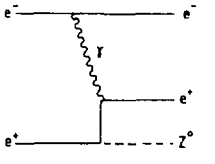

The corresponding cross section is about 3pb at $E_b = 100$ GeV. Low masses for the $Z_0 e_2$ system, close to threshold, are favoured. The Z^0 takes essentially all the beam energy and the

remaining electron e_2 has a low momentum. This gives very asymmetric final states with large missing energy.

2.2.3 Single W production

In the same way, single W bosons can be produced by "γe interactions. The cross section is much smaller than in the previous case, being ~ .4pb (E_b = 100 GeV). In contrast to the previous reaction, this process favours large W-ν masses, close to the kinematical limit.

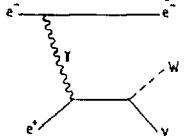

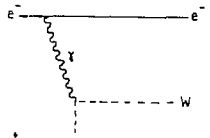

The direction of the produced W is peaked along the beam.

2.3 W and Z pair production[3]

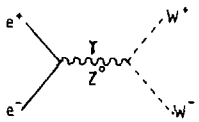

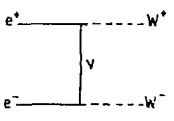

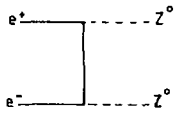

The reaction $e^+e^- \rightarrow 4$ fermions, with intermediate formation of W and Z bosons is the dominant mechanism for W and Z production. Depending on the final state, W and Z mediated amplitudes can interfere. This effect is in practice very small and has been neglected in this study. At E_b = 100 GeV, the Z^0 pair production is about 6% of the W pair cross-section which amounts to 15pb. The rise of the cross section with energy is determined by the values of the W mass and width and also by radiative corrections.

On fig.1 we have shown the contribution of the various mechanisms for different beam energies and in the following we will consider only the pair production of W bosons.

3. THE THEORETICAL W MASS SPECTRUM AT THE PARTON LEVEL AND THE EFFECT OF RADIATIVE CORRECTIONS

3.1 W line shape without radiative corrections

We forget for a moment the presence of radiative corrections and consider the W production at $\sqrt{s}$ = 130 GeV. Several effects can distort the W mass line shape in comparison to a simple Breit-Wigner dependance of the form :

$$BW(M)\,dM = \frac{A}{(M^2 - M_0^2)^2 + \Gamma_0^2 M_0^2}\,dM \qquad (1)$$

3.1.1 The decay matrix elements of the W depend on the actual W mass

$$\mathcal{M}^{\text{decay}} \sim M\, f(\text{angles})$$

and as the cross section varies like :

$$d\sigma \sim \left| \mathcal{M} \right|^2 dM^2$$

we expect that the parameter A in (1) varies with M like :

$$A = A_0 (M/M_0)^2$$

In practice $A = A_0(M/M_0)$ gives the best adjustement of (1) to the generated parton-parton mass distribution. With this dependance, the fitted W mass is close to the input value within 4 MeV (with an accuracy of the similar order) whereas a cubic behaviour for A gives a displacement by 40 MeV. This result happens to be due to a cancellation mechanism generated by the interference of different W helicity amplitudes[4].

3.1.2 Because of radiative corrections to the W propagator[5] the W natural width depends on the actual vector boson mass. We expect to have $\Gamma(M) = \Gamma_0\, M/M_0$. If we use this behaviour during the event generation and if we keep the expression (1) which neglects this effect, the fitted mass is lower than the nominal value by 20 MeV.

3.1.3 In the process of W mass reconstruction we will impose, as a constraint, the equality between the energies of the beam and of the W. In practice this is never true because the two emitted W's have different masses. The adjustement of expression (1) gives a fitted value which is 25-35 MeV higher than the original mass.

3.2 Effect of radiative corrections

The complete hard photon emission cross-section, involving the diagrams shown on fig. 2, has been calculated[6] and will be available as an event generator. These computations are needed for an accurate determination of the W mass using real data. In the following we have only considered the effect of the initial state radiation which represents the bulk of the contribution.

Radiative corrections decrease the slope of the energy variation near threshold of the W pair production cross-section.

They can also distort the W mass distribution by reducing the available phase space for W production. This effect is marked near threshold but is negligible for E_b = 95 GeV (displacement $\Delta M \sim$ a few MeV).

The largest effect of radiative corrections comes when we use the beam energy constraint (Cf. following paragraph) because we overestimate the real available energy used to produce W pairs and thus we create a tail at high W masses. The fitted value is displaced by 470 MeV (± 40 MeV) and this value depends slightly on the interval used for the adjustment (fig. 3).

At this stage of the study we can reproduce, using a Monte Carlo program, the exact shape of the W mass distribution with an accuracy well below 50 MeV. This situation is a characteristic of e^+e^- machines.

4. BACKGROUND OF THE W^+W^- CHANNEL AND ITS REJECTION

Cross sections for most of the processes occuring in the LEP II energy range, not including radiative corrections, are shown on fig.4. The decays of pairs of W or Z bosons are not the main sources of hadronic events at E_b = 95 GeV. Hadrons are essentially produced in e^+e^- annihilation events into $q\bar{q}$ pairs or in $\gamma\gamma$ collisions. Most of the events are coming from radiative corrections, this means that the mass of the hadronic system is smaller than the total available energy and that there is usually a bad energy balance between the initial and final measured states.

4.1 Cross sections (fig.5)

4.1.1 Photon-photon interactions

The hadronic cross section in $\gamma\gamma$ collisions depends sharply on the mass of the produced hadronic system. For instance, if we require that $M_{had} > 0.4\sqrt{s}$, the total cross section for $q\bar{q}$ production is of the order of 1 pb at $\sqrt{s}$ = 190 GeV. Thus in the following, the contribution from this process will be neglected.

4.1.2 Annihilation events

At the same energy, the total hadronic annihilation cross-section is 23 pb in the absence of t quark production and without including radiative corrections. The radiative corrections push this value up to about 100 pb. The cross section for events of the type $e^+e^- \to \gamma Z^0 (\gamma)$ where $\hookrightarrow q\bar{q}$ the high energy photon is seen in the apparatus ($\theta_\gamma > 10°$) amounts to about 16 pb.

4.2 Background rejection and selection of the W^+W^- channel

Our aim being to measure the W mass, we have only considered events in which, at most, one W decays leptonically. These events can be characterized by the following properties :

- about equal energy sharing between the two W's. Each W has an energy close to the beam energy and large radiative emissions are depressed by the sharp energy variation of the production cross-section.
- each hadronic decay of a W gives at least two energetic jets.
- a leptonic decay generates a high energy charged lepton $E_\ell > 20$ GeV

(at $\sqrt{s}$ = 190 Gev..

We have to consider two classes of events according to the presence or not of a W leptonic decay.

4.2.1 Background to the channel $W_{1,2} \to$ hadrons (fig.6)

We have to eliminate most of the radiative events. An energy balance cut is not sufficient because a lot of the radiated energy can be seen in the apparatus. Such events can be characterized by the presence of an isolated γ or by an e^+e^- pair of high energy. Sometimes the photon is included in an hadronic jet by the cluster finding algorithm and this usually gives a jet with a leading high energy photon.

We have required a minimum number of 4 reconstructed jets. This notion of jet is cutoff dependant during the generation of the events and also depends on the algorithm during the reconstruction. Most of the events in the background have in fact three generated QCD jets but the algorithm has splitted one of the jets in two parts providing a four jets event. We have merged two jets if their relative angle satisfies $\cos\theta_{ij} > .8$. This cut keeps more than 90% of the $W\bar{W}$ events and removes 50% of the background.

We then ask for energy balance in two steps :

- we require a two jets combination with an energy close to the nominal beam energy within 10 GeV.

- we demand that the missing energy of the remaining system will be less than 30 GeV to ensure a rough global energy balance.

These cuts, defined at $\sqrt{s}$ = 190 GeV, have an efficiency of 75% on W events and keep only 0.7% of the background.

4.2.2 Background to the channel $W_1 \rightarrow \ell\nu$, $W_2 \rightarrow$ hadrons (fig.7)

We ask for a high energy lepton ($E_\ell > 20$ GeV). This eliminates the main part of the W decays into $\tau\nu$, and a particular selection has to be defined to recover these events[7].

The background is mainly coming from events in which a high energy photon is converted inside the apparatus. For instance, the gamma produced in γ-Z_0 events. A good rejection against electromagnetic pairs has to be provided by the detector, which can be achieved easily with dE/dX information.

The remaining background comes from semi-leptonic decays of heavy flavours and can be reduced by a cut on the lepton isolation. For instance, we can ask for no track with more than 2 GeV in the jet which contains the lepton. Such a cut is also efficient against "muon" candidates from hadronic punch-through. On fig.7 we have shown the effect of a cut on energy balance between the beam and all the hadrons seen in the apparatus. If events are selected using the condition $-5\ \text{GeV} < E_{beam} - E_{hadrons} < 10\ \text{GeV}$ we can remove essentially all the background.

The level of background for this channel becomes negligeable, well below 1 pb.

5. W MASS MEASUREMENT FROM THE THRESHOLD BEHAVIOUR OF $\sigma(e^+e^- \rightarrow W^+W^-)$

The lowest order cross section for $e^+e^- \rightarrow W^+W^-$ [3] grows very fast near threshold. The finite width of the W will of course greatly reduce the sensitivity of the total cross section to the W mass. However, a first study on the feasability of the W mass determination from the measurement of the W^+W^- pair production cross section showed that a statistical error on M_W below 100 MeV was within reach[8].

In contrast to the other methods (where one would like to run at the maximum of the production cross section), this method needs some luminosity around the threshold region. However, in a scenario where the upgrading to full LEP II energy is done in steps, the required lower beam energies will in any case be available for some time.

The method is based on a least squares fit of the expected cross sections at different energies to the measured cross sections for W^+W^- production. A precise knowledge of the

theoretical cross section is therefore essential. In particular, radiative corrections and finite width of the W have to be taken into account. From the experimental side, the detector efficiency (as a function of the beam energy) has to be known with sufficient precision.

5.1 Statistical Procedure

The excitation curves are calculated numerically. They can be compared to Monte Carlo integration of the full matrix element for W pair production and their subsequent decay into 4 fermions[9]. This part of the event generator includes hard photon radiation by one of the incoming electrons ($E_\gamma > 0.1$ GeV) and the width of the W ($\Gamma = 2.65$ GeV). The results are shown in figure 8, using $M_W = 82$ GeV and $\sin^2\theta_W = 0.223$.

It is now assumed that at N energies E_i the total W pair production cross section σ_i is measured, from runs with integrated luminosity L_i. The total integrated luminosity ΣL_i was fixed at 500 pb^{-1}. The values of σ_i were drawn from curves like in Figure 8 + (optionally) a background contribution σ_{bg}, parametrized as a+ b/s. These 'experimental' cross section values σ_i were then smeared according to an rms spread of $\sqrt{\sigma_i/L_i}$. The N values σ_i are then used in a least squares fit to the theoretical excitation curve and a 'best' value of M_W is obtained. This 'experiment' is repeated say 1000 times. The expected error σ_M on the mass measurement from a single experiment is then obtained from the rms value of the distribution of these 1000 M_W values.

5.2 Optimization of data taking

Assuming an integrated luminosity of 100 pb^{-1} at each energy, figure 9.a shows the absolute value of the difference between the cross sections obtained for two different W masses (82 and 81.9 GeV) divided by the expected r.m.s. error. This quantity, called resolving power, has a peak at about 82 GeV, is zero at 86 GeV where the two cross sections are equal, and increases again for higher energies because the cross section rises to a higher plateau for higher W masses. Therefore the energy settings should be concentrated around the nominal W mass, M_W = 82 GeV, and at much higher energies, above 92 GeV. The cross over region between 84 and 88 GeV should be avoided.

This is demonstrated in figure 9.b. Data taking is always distributed over five energies. The two points at 75 and 95 GeV are fixed. The low energy point is essential for background determinations and the higher one is at the highest available energy. Several ways to order the remaining three energies are shown in figure 9.b. The best precision attainable for the W mass is σ_M = 90 MeV. This result holds for a variety of energy settings as long as no luminosity is wasted in the region of 84 to 88 GeV.

The presence of a (small) constant background contribution of 0.2 pb would already lead to a systematic shift on the W mass of ~ 130 MeV if one would not allow for a background term in the fit to the excitation curve. Considering 5 cross section measurements at 75, 95, E and E ± 1 GeV, whith the same luminosity of 100 pb^{-1} at each point, we have plotted in figure 10 the variation of σ_M which the energy E for different background contributions :

1. solid curve : no background,
2. dashed curve : background = $2.0 \times \frac{10^4}{s^3}$ [pb] (i.e. 9.74 pb at 82 GeV),
3. dashed-dotted curve : background = $4.0 \times \frac{10^4}{s^3}$ [pb] (i.e. 1.5 pb at 82 GeV).

Figure 10a is the result from fits that include a background parametrization as $\frac{b}{s}$, whereas Figure 10b corresponds to fits with background terms $a + \frac{b}{s}$.

From Figure 10a one can conclude that with reasonable assumptions about the background, a statistical error on M_W of 120 MeV can be obtained. The presence of an additional constant background term of 0.5 pb would give a systematic mass shift of ~60 MeV.

5.3 Systematic errors

The statistical errors on the cross section measurements, even when using all the events, range between ~2.5 % at 95 GeV and > 10% at 75 GeV. It is therefore clear that anticipated point-to-point uncertainties on the luminosity of 2% will have a negligible effect on the final mass resolution. An absolute uncertainty of 5% on the luminosity leads to a systematic error on the W mass of 120 MeV.

The same argument holds with respect to the knowledge of the detector efficiency. Its absolute value has to be known within a few percent to keep the resulting systematic error small compared to the expected statistical error. As the W production angular distribution becomes more peaked in the forward direction at higher energies, the loss of events due to the hole in the detectors around the beam direction is expected to be energy dependent. However, from Monte Carlo calculations it was found that this energy dependence over the range 75 to 100 GeV is small. When neglected in the fit, the additional systematic error on M_W was < 10 MeV.

5.4 Conclusions

A fit of the theoretical excitation curve for W pair production to the measured cross sections at 5 different energies with an integrated luminosity of 100 pb^{-1} at each energy, allows to extract the W mass with a statistical error between 100 and 130 MeV. This result is obtained using all events and under the assumption that the background has a known 1/s shape (one free parameter) and is < 1 pb at 83 GeV. If a second parameter is needed to describe the background, the error on the W mass becomes 170-190 MeV. It would then be better to use only events where one (or both) of the W's decays leptonically. The background is expected to be much smaller. In that case, the statistical error on M_W will be ~130 MeV.

6. W MASS RECONSTRUCTION USING THE W DECAY PRODUCTS

During the LEP workshop in Les Houches in 1979[10] it has been proposed to identify the W particles using the mass of the two jets produced in the final state. The peak obtained this way is broad and displaced towards low masses because all the particles are not measured in the apparatus.

The accurate mass measurement of the D and B particles[11] produced in pairs at $e^+ e^-$ colliders, is obtained after imposing the equality of the beam and particle energies. We will show in the following that a similar technique -quoted as "mass rescaling"- can be applied to W bosons.

After a study of the jet energy reconstruction in typical LEP detectors we detail the properties of "mass rescaling". The W mass measurement is then considered for hadronic and leptonic decays. In these Monte-Carlo studies events were always generated with a "true" W mass of 82 GeV. The understanding of systematic mass displacements is finally presented.

6.1 Measurement of the events

Particles produced in the final state are distributed among a few jets. The 4-vector energy-momentum of these jets can be obtained using the energy deposited in calorimeter cells (hadronic and electromagnetic) or by reconstructing individual particles making use of the fine granularity of LEP detectors. These detectors have been designed to do measurements at the Z^0 pole. At LEP II the energy is 2 times higher but in case of W pair production we have also 2 times more jets in the final state which means that the detectors are also well conceived for this energy domain. In table I are given typical detector parameters used for this study.

6.1.1 Calorimetry[12]

We have considered the best calorimeter designed for LEP (L3 detector). Hadrons loose 40 ± 20 % of their energy in the BGO with an e/π response of 1.4. No attempt has been made to distinguish electromagnetic from hadronic showers in the BGO. The total measured energy of the jets is then : $E_{meas} = f_{BGO} \times E_{BGO} + E_{HCAL}$ with $f_{BGO} = 1.15$ determined empirically by Monte Carlo.

The detection threshold for photons in the BGO is very low (30 MeV) and the main distorsion induced between the real and measured energy comes from :

- detector holes along the beam directions (2% of 4π)
- escaping neutrinos ($E_\nu \sim 3\%$ of the jet energy)
- difference in response of the electromagnetic calorimeter to photons and hadrons.

6.1.2 Individual hadron reconstruction

Charged hadrons are measured in tracking devices with a better accuracy than in an hadronic calorimeter.

Photons and neutral hadrons are measured using electromagnetic and hadronic calorimeters. Some of them are lost because a charged hadron may have started a shower in their neighbourhood. These losses depend on the granularity of the calorimeters. With an appropriate algorithm we can reduce their importance. For instance we can measure the energy of a charged track in the following way :

$E = E_{TPC}$ if $E_{TPC} - E_{EM} - 1.5\,\sigma_E + E_{HCAL} - 1.5\,\sigma_H$

or $E = E_{EM} + E_{HCAL}$ if this condition is not satisfied.

Apart for the L3 BGO calorimeter, visibility thresholds for electromagnetic and hadronic showers are not usually negligible and we have done a study using 500 MeV for photons and 1 GeV for neutral hadrons.

6.1.3 Mean reconstructed energy, E_{meas}

Whereas for the L3 calorimeter, the difference between the mean reconstructed energy and the jet energy can be attributed to escaping neutrinos (3%), for other detectors it amounts to about 10 %. The corresponding distribution is given in fig. 11 and is very asymmetric.

Two classes of events can be defined :

- those situated in the tail for which, usually a high energy particle has been lost (photon or neutral hadron in the jet core),

- those situated around the peak value (5% of energy loss) for which the energy lost is determined mainly by threshold effects and escaping neutrinos.

6.1.4 Energy resolution = σ_E

In case of calorimetric measurements the jet energy resolution is given by the energy resolution of the hadronic calorimeter.

For granular devices the variance of the reconstructed energy distribution is determined by the tail and corresponds to a similar accuracy. If we consider only those events situated around the peak value and use the FWHM of the distribution to estimate the energy resolution we get an improvement by a factor ~2.

On fig.12 we have shown the variation of $\langle E_{meas} \rangle$ and σ_E with the jet energy. Apart for jets emitted in the very forward and backward directions, we have not observed a real variation of these quantities with the jet polar angle.

6.1.5 Reconstructed mass for hadronic decays

Two classes of events have to be considered :

- class -1 : one W decays leptonically

- class- 2 : the two W's decay into hadrons.

These events have to fulfil the conditions imposed on background rejection.

For class-1 events all hadrons are supposed to come from the W decaying non leptonically. For class-2 events we have to use an algorithm to attribute a jets subsample to a given W decay. In this case we have only considered events with 4 or 5 jets reconstructed in the final state using the standard LUND algorithm LUCLUS[13] and we have assumed that one of the W's has decayed into 2 jets. This jet-jet combination is obtained requiring that the difference between the jet-jet energy and the beam energy is minimal. The remaining hadronic system is attributed to the other W.

The reconstructed mass-spectra are shown on fig.13 and 14 for class-1 and class 2 events respectively. The peak position is lower than the nominal W mass by a few GeV because of energy lost during the event reconstruction and the width of these distributions is of the order of 10 GeV.

6.2 Mass rescaling using the beam energy

We propose to scale the measured W mass by the ratio of the beam and W measured energies.

$$M = M_{meas} \times \frac{E_{beam}}{E_{meas}} \qquad (2)$$

This expression can be justified by the following arguments. If we lose one particle belonging initially to one of the two jets from a W decay : the difference between the measured W mass and the initial value is coming from :

- a variation of the two jets opening angle,

- a decrease of the energy of one jet.

The relative jet-jet angle is very large (~100°) and its variation will be of the order : $\delta\theta \sim P_t / P_{jet}$, thus $\delta\theta/\theta$ is very small and the corresponding variation of $\delta M \sim 100$ MeV.

The effect of energy loss is much more important. If we define $z = P/P_{jet}$ (P = particle momentum) the induced variation on the W mass will be : $\Delta M \sim z \times M/2 \sim P$.

The reconstructed W mass spectrum reflects the energy containement of the detector.

If we forget for a moment, the presence of radiative corrections and the unequality of the two W masses we can impose the equality of the beam and W energies and, in the case of pure hadronic decays, the balance between the W momenta. Such a fitting procedure can be done, knowing the jet energy and angle reconstruction accuracies of the detector (cf. fig.11). As the mass displacement is dominated by escaping energy we have only corrected for this effect and if we assume that the jet energy reconstruction obeys the relation :

$$\frac{\sigma_E}{E} = \frac{A}{\sqrt{E}}$$

we get the expression (2).

The mass distributions obtained this way are shown also on fig.13 and 14 and have the following properties :

- the distributions are narrower by a factor 2, their width is about 2 times the W natural width.

- they are about centered at the nominal W mass (if we do not consider for a moment the effect of radiative corrections)

$M = M_0 - 200$ MeV (L3)

$M = M_0 - 300$ MeV (Delphi)

In the following we show that the fitted position of the W reconstructed mass is not very sensitive to the expected detectors properties and to the hypothesis used in the simulation.

A similar approach has been proposed to reconstruct the mass of heavy particles decaying into a few jets system produced in $e^+ e^-$ annihilation : top mass, gluino mass[9]...

6.3 Reconstruction of the W mass when W → hadrons

6.3.1 Typical statistics and background

For class-1 events, after background rejection cuts, but without requiring energy balance and using an integrated luminosity of 500 events/pb we will get 3000 hadronic W decays.

For class-2 events, after all cuts we have 1700 events (in the mass peak).

The background in the mass plots from non W events is negligible and structureless (fig.15).

6.3.2 Calorimetric approach

We use only class-1 events (fig. 16a).

The mass distribution is asymmetric with a tail towards high masses because of radiative emissions. A Breit-Wigner distribution added to a second order polynomial background is adjusted on the "data". This gives

$M = 82.273 \pm .065$ GeV

6.3.3 Granular detector approach

With class-1 events, a similar spectrum is obtained, the fitted mass beeing M = 82.17 ± .060 GeV. This value is 100 MeV lower than the previous one in agreement with the result given in 6.2 where, because of higher energy losses than in the calorimetric approach, the mass without radiative corrections is already lower by 100 MeV.

If we impose a cut on energy balance (at 10 GeV) the tail at high masses is reduced and we get :

$$M = 82.020 \pm .060 \text{ GeV}. \quad \text{(fig.16-b)}$$

(this value is obtained adding the W → hadrons and W → ev mass distributions).

Using class-2 events (fig.16-c) we get similar results, the signal is sitting on a flat "background" coming from wrong assignements of 2 or 3 jets combinations.

6.4 Reconstruction of the W mass in case of leptonic decays

We consider class-1 events.

The direction of the neutrino was calculated from the momentum vectors of the lepton and the hadronic system

$$\vec{P}_\nu = \vec{P}_{miss} = -(\vec{P}_{hadr} + \vec{P}_\ell) \qquad (3)$$

In reconstructing the $\ell\nu$ mass two possibilities were tried to improve on the resolution. In the first method the ν energy was calculated from equation (3) imposing the beam constraint $E_{hadr} = E_b$. This results in mean mass values slightly below the nominal W mass. In a second approach the ν energy was calculated constraining the $\ell\nu$ system to the beam energy using $E_\nu = E_b - E_\ell$. The lepton energy was not rescaled since it is measured with much higher accuracy than the missing energy. This method gives mass values slightly above the nominal W mass and also results in narrower ($\ell\nu$) mass distributions.

The statistics amounts to about 1200-1300 W → ev + μν events and we obtain the following results :

$$\text{method 1 : } M = 81.84 \pm .12 \text{ GeV}$$

$$\text{method 2 : } M = 82.38 \pm .09 \text{ GeV}$$

The corresponding mass distributions are given in fig.17.

6.5 Stability of the W mass measurement

The reconstructed W mass has not exactly the nominal value. The largest displacement is due to radiative corrections and is well under control. The other source of displacements comes from the reconstruction procedure, their magnitude is at most 300 MeV and we have studied the dependence of these displacements on the hypothesis used in the simulation.

We have thus generated a large event sample to get a sufficient statistical accuracy. Using the nominal values of the expected detector performances we obtain a reconstructed W mass of : M = 82.037 ± .030 GeV and we study deviations from this value.

6.5.1 Bad knowledge of detector calibration

If we assume, in a complete non realistic way, that the hadron energies are measured 3% higher than their exact values whereas photons have an energy 5% lower we obtain :

$$M = 82.137 \pm .031 \text{ GeV}.$$

This effect has to be correlated to the displacements observed after mass rescaling where $\Delta M \sim -200$ MeV for a mean energy loss of 3% and $\Delta M \sim -300$ MeV for a loss of 5%.

If we want to keep these shifts below 100 MeV, the absolute detector calibrations must be known with an accuracy better than 2 %.

We must note that, because of the rescaling procedure, our measurement is not affected by a common miscalibration of the hadronic and electromagnetic calorimeters.

6.5.2 Increase of the overlap probability between showers in case of granular detectors

The algorithm given in 6.1.2 is stable relative to this parameter. But if we consider that photon or neutral hadron initiated showers are lost because of the presence of a nearby hadronic shower we increase the mean energy loss.

For instance, if we multiply by 1.5 the minimum distances below which two showers are merged, we double the probabilities to lose such particles and their values become : 6% for photons and 38% for neutral hadrons.

The fitted mass is then : M = 82.012 ± .046 GeV.

6.5.3 Presence of the $t\bar{b}$ decays

Up to now we have assumed, in the case of pure hadronic final states, that the top quark mass is so heavy that no decay of the W was possible into the $t\bar{b}$ channel. If we take a top quark mass of 35 GeV the main effect is to decrease by ~25% the number of reconstructed W's appearing in mass peaks.

M = 81.936 ± .036 GeV

6.6. Need for a Monte Carlo program

This program has to correct for displacements of the mass of amplitude ~200-300 MeV with an accuracy better than 100 MeV.

It must incorporates radiative corrections and detector response. This program does not require a very high level of sophistication as the one needed to search for rare events which has to reproduce some marginal behaviour of ordinary events. In our case we are concerned by the mean response of the apparatus.

The simulation of the energy reconstruction in the apparatus can be tuned using hadronic events registered at the Z_0 pole (a few 10^6 events).

At LEP II the process $e^+e^- \rightarrow \gamma Z^0$ offers, with similar statistics as the production of W pairs and in the same experimental conditions, a measurement of the Z^0 mass. In addition to Bhabha events the high energy "monochromatic" photon gives also an absolute calibration for the E.M. calorimeters.

The constraint $E_z{}^0 = 2E_{beam} - E_\gamma$ can be imposed to rescale the Z^0 reconstructed mass and we obtain a statistical accuracy of ~70 MeV on the Z^0 mass, fig 18.

7. W MASS RECONSTRUCTION FROM THE END POINT OF THE LEPTON ENERGY SPECTRUM

The lepton energy spectrum from the two body decay $W \rightarrow \ell\nu$ can be directly related to the W mass. In the laboratory frame the kinematical limits w_- E_ℓ $< w_+$ are given by the Lorentz boost of the W :

$$w_{\ell} = E_W \times \frac{1 \pm \beta}{2}$$

In addition to detector resolution effects the limits are smeared by the finite W width and QED photon radiation. This is particularly important for the low energy limit with additional background from τ decays. To have the best sensitivity from this technique we need very good lepton energy resolution so that the smearing from the apparatus response will be smaller than the natural smearing. This impose :

$\sigma_p / p < 2 \times 10^{-4}\ p$ if tracks are measured by their curvature

or $\sigma_E / E < .12/\sqrt{E}$ if a calorimeter is used.

These conditions can be fulfilled only by the L3 BGO calorimeter for which the expected electron energy resolution is 0.6% at 70 GeV.

The simulated electron spectrum for $M_W = 82.0$ GeV is shown in fig. 19. *The analysis was done* by generating data sets with ~30 fold statistics for different M_W values in steps of .25 GeV and then perform a χ^2 fit to the "measured" spectrum. To get a feeling of the sensitivity fig. 20 shows a detailed view of the measured end point spectrum compared with the predicted spectra for 81, 82 and 83 GeV. The data start to become different only at $E_\ell > 65$ GeV, which contain only 20% of all electrons.

The result of the analysis gives $M_W = 81.7 \pm 0.3$ GeV, where the error is completely dominated by statistics (1000 events in the whole spectrum). If the energy resolution is assumed to be a factor 2 worse, then the result is $M_W = 82.3 \pm 0.5$ GeV.

In this kind of analysis a careful energy calibration is crucial. A calibration error directly reflects in the mass determination, e.g. a miscalibration by 1% induces a mass shift of ~0.7 GeV.

8. W WIDTH MEASUREMENT

Using class. I events we studied the width of the fitted mass distribution as function of the intrinsic W width. As shown in figure 21 there is a linear relationship which can be approximated by:

$$\Gamma_{rec} = \Gamma_W + 2.8\ \text{GeV}$$

A determination of the W width seems possible with a typical precision of 200 MeV, a value comparable to the contribution from one leptonic channel (e.g. $W \to e\nu$) in the standard model.

9. W MASS MEASUREMENT AT $p\bar{p}$ COLLIDERS

P. JENNI has given at this workshop the expected accuracy on W mass determination after the upgrading of UA1 and UA2 experiments.

As in a $p\bar{p}$ collider one cannot apply the "mass rescaling", the jet-jet decays cannot be used for an accurate mass measurement and only the ratio or the difference between the W and Z masses can be obtained with some accuracy.

In our group we have studied the theoretical uncertainties on the W mass reconstruction[15].

The W mass will be obtained from an adjustment of a theoretical expectation to the distribution of a measured variable which can be the transverse energy of the lepton. Such expectations require an elaborated QCD computation which will be tuned on other measurable quantities obtained in the same experimental conditions.

The theoretical uncertainty is actually estimated to be :

$$\frac{\delta M_W}{M_W} \sim \frac{300 - 400\ \text{MeV}}{M_Z}$$

10. THEORETICAL INTEREST IN MEASURING M_W AT THE 1% LEVEL

10.1 Introduction

A test of the electroweak theory beyond the tree level with high precision measurements at LEP-I, SLC, ACOL, Tevatron, HERA and LEP-II could confirm the range of validity of the standard model and/or could signal the need for significant modifications either in the Higgs-sector or in the fermion and gauge boson sector.

The experimental basis for such a quantitative test are (or will be) precise measurements of the ratio of neutral to charge νN and νe scattering, of the mass values of the Z and W bosons, their widths, and of various asymmetries (charge asymmetry, longitudinal and transverse polarization asymmetry) on the Z^0 resonance. At the one-loop level, all radiative corrections have been computed including the polarization asymmetries[8].

It turns out that the bulk of the radiative corrections are contained in two easily calculable effects[6] :

i) change in the scale in the definition of the renormalized coupling $\alpha(m_e) \to \alpha(m_Q)$[25]

ii) vacuum polarization effects for the massive gauge bosons (dominated by heavy fermions or scalars).

This allows to incorporate the radiative corrections in the following suggestive order[6] :

a) tree level results.

b) effective Born approximation : the effects i), ii) can be included by simple redefinition of the respective quantities in the (leading) tree results. This approximation is exact enough to discuss all measurements mentioned above, except the W-mass measurement proposed here.

c) inclusion of the remaining calculations of the Standard Model (Box-diagrams, etc). The effects of most particles beyond the standard model can be incorporated in b) ; their effects in c) are presumably always very small.

In models with non-standard Higgs content the so called ρ-parameter may be different from one already at tree level. Since, experimentally $\rho \simeq 1$, and the radiative corrections to ρ coming from vector boson self energies are already included under b), we can use the tree level expression, conveniently written as :

$$\rho = 1 + \Delta\rho \ , |\Delta\rho| \ll 1$$

to include such effects. Then, all data can be written, up to the corrections under c) in terms of Δρ and the corrections of b).

10.2 Radiative corrections

10.2.1 Standard Model

The Standard Model contains three parameters in the gauge sector testable at LEP II*. It is best to choose them to be the precisely known quantities :

$$\alpha^{-1}(m_e^2) = 137.035963\ (13) \text{ (from the Josephson effect)} \quad (1)$$

$$G_F = (1.16634 \pm 0.00002)\ 10^{-5}\ \text{GeV}^{-2} \text{ (from muon decay including QED corrections)} \quad (2)$$

along the Z-mass which will be known with an accuracy of about 1/20 %. Its present value is :

$$M_Z = 93 \pm 3\ \text{GeV} \quad (3)$$

All other quantities are expressed in terms of these three, including $S^2 = \sin^2\theta_W$. At tree level

$$S^2 = \frac{1}{2}\left(1 - \sqrt{1 - \frac{4\,\mu_e^2}{M_Z^2}}\right) \quad (4)$$

$$M_W^2 = \frac{M_Z}{2}\left(1 + \sqrt{1 - \frac{4\,\mu_e^2}{M_Z^2}}\right) \quad (5)$$

with

$$\mu_e^2 = \frac{\pi\,\alpha(m_e)}{\sqrt{2}\ G_F} = (37.281\ \text{GeV})^2 \quad (6)$$

The one-loop radiative corrections modifies these results. Since the quantity S^2 is not free anymore, it is expressible in terms of the basic three parameters. Its value depends on the particular experiment chosen to define it**[3], different definitions differ by radiative corrections which are small after the step b) above has been taken. We choose

$$S^2 \equiv (1 - C^2) = \left(1 - \frac{M_W^2}{M_Z^2}\right) \quad (7)$$

advocated by Sirlin[17].

Now, all radiative corrections at the one-loop level can be parametrized by letting

$$\mu_e^2 \to \mu_e^2 / (1 - \Delta r) \quad (8)$$

where Δr contains one-loop corrections due to known and unknown particles. Δr has been evaluated in[17] in the Standard Model and by later authors also for other models[18]. Setting the unknown parameters

$$m_t = 36\ \text{GeV} \quad (9)$$

* Excluding the mass of the Higgs boson whose effects will be seen to be weak.

** S^2 is usually defined by an experiment in the same way as the tree level relation reads for the particular experiment.

$$m_H = M_Z \tag{10}$$

one gets

$$\Delta r = 0.0696 \pm 0.002 \tag{11}$$

with an uncertainty due to hadronic corrections[24].

About 85% of (11) are accounted off by the change in α.

10.2.2 Extensions of the Standard Model with $\rho \neq 1$

As mentioned, with an expanded Higgs sector, $\rho \neq 1$; instead

$$\rho = \frac{2 \sum_i \langle v_i \rangle^2 \left(I_i^2 + I_i - \frac{3}{4} Y_i^2 \right)}{\sum_i \langle v_i \rangle^2 Y_i^2} \tag{12}$$

at tree level. In (12), the v_i, I_i and Y_i are the v.e.v.'s, isospins and hypercharges of the Higgs fields Φ_i, over whom the sum runs. For any number of doublets, $\rho = 1$; for one doublet D and one triplet T :

$$\rho = \begin{cases} 1 + \dfrac{4 v_T^2}{v_D^2} & Y_T = 0 \qquad (13) \\ 1 - \dfrac{2 v_T^2}{v_D^2 + 4 v_T^2} & Y_T = -2 \qquad (14) \end{cases}$$

Experiments imply $v_T^2 / v_D^2 \ll 1$.

Eqs (4) and (5) are now modified. Using the gauge invariant renormalization condition*

$$M_W^2 = \rho \, c^2 M_Z^2 \tag{15}$$

where ρ is set equal to its tree level value, one obtains

$$S^2 = \frac{1}{2} \left(1 - \sqrt{1 - \frac{4 \mu_0^2}{\rho M_Z^2 (1 - \Delta r)}} \right) \tag{16}$$

$$M_W^2 = \frac{1}{2} \rho M_Z^2 \left(1 + \sqrt{1 - \frac{4 \mu_0^2}{\rho M_Z^2 (1 - \Delta r)}} \right) \tag{17}$$

* This condition generalizes (7) introduced by Sirlin[21].

Writing, as suggested above, $\rho = 1 + \Delta\rho$, we see clearly how Δr and $\Delta\rho$ enter in a similar way. Neglecting corrections c) (usually less than 10 % of the total corrections), Δr and $\Delta\rho$ are the same for all experiments analyzed in the effective Born approximation b) and conveniently sum up the effects of m_t, m_H and the new physics.

(15) and (16) now allow to test the Standard Model (with $\rho = 1$ and Δr given in (11)); similarly new physics changes Δr and $\Delta\rho$. Changing $\Delta\rho$ and Δr by $\delta\Delta\rho$ and $\delta\Delta r$, we obtain for the shifts in the measured values of S^2 and M_W^2 :

$$\delta S^2 = \frac{S^2 C^2}{1 - 2S^2} (\delta\Delta\rho - \delta\Delta r) \qquad (18)$$

$$\delta M_W^2 = \frac{M_Z^2 C^2}{1 - 2S^2} (C^2 \delta\Delta\rho - S^2 \delta\Delta r) \qquad (19)$$

It is remarkable that in (18) and (19) $\delta\Delta\rho$ and $\delta\Delta r$ enter with different linear combinations.

It is important to note that all the precision asymmetry measurements on the Z^0 resonance mentioned are sensitive only to S^2, that is to :

$$(\delta\Delta\rho - \delta\Delta r) \qquad (20)$$

at the leading level (i.e. excluding corrections c)) since they depend on ρ only via S^2.

This is true also for the measurement of the ratio of the cross-sections for $\nu_\mu e$ and $\bar{\nu}_\mu e$ interactions.

On the other hand, the ratio of neutral to charged ν_μ interactions on isoscalar targets has also a different dependance on $\Delta\rho$ and Δr.

On figure 22 we have drawn to contour lines expected from the various experiments. The interest for a W mass measurement at the 1‰ level is two folds :

- it provides an independant measurement with the same accuracy as LEPI on Δr,
- it is the most sensitive (5 times) to deviations from $\rho = 1$.

10.3 Effects of new particles on M_W

A shift $\delta\Delta r$ of Δr (due to new physics) displaces M_W by an amount δM_W which, according to (19) is given by :

$$\frac{\delta M_W}{M_W} = + \frac{S^2}{2(1-2S^2)} \delta\Delta r \simeq - 0.2\, \delta\Delta r \qquad (23)$$

where we have assumed the new particles not to change $\rho = 1$ at the tree level. It is now interesting whether new particles can give rise to a measurable $\delta M_W / M_W$ (i.e. which exceed 1 ‰). The following results have been obtained :

10.3.1 Heavy top quark[9].

If m_t exceeds the "standard" value of 36 GeV, one obtains the following shifts in M_W ($m_H = M_Z$):

m_t(GeV)	36	60	100	150
δM_W(MeV)	0	-30	220	500
$\delta M_W/M_W$	0	0.0004	0.003	0.006

If we assume, the measured value of M_W to fall onto the "standard value", this allows a bound on $m_t \lesssim 80$ GeV in the experiment (assuming no other new physics !).

10.3.2 Additional heavy quarks and lepton doublets[18-19]

If the two members of the doublet have very different masses, the shift in M_W is larger than 1 ‰ for quarks and 0.0006 (m^2_{lepton}/m_Z^2) for leptons. In view of the asymptotic validity of these results, such doublets could be excluded. If the masses are degenerate, however, then one get $\delta M_W = -14$ MeV and - 42 MeV (leptons and quarks, respectively). A 1 ‰ measurement would limit the number of additional generations to about 7-8 and 2-3.

10.3.3 Supersymmetric particles[18-20]

The effects of supersymmetric partner doublets of the quarks and leptons are the same as under 10.3.2 if the particles are heavy, as usually expected. Since in many models the Squarks and Sleptons have a large common mass $m^2_{\tilde{\gamma}/z}$ with mass differences $\sim m_{\tilde{\gamma}/z}$ (Δm quark), the large effects due to very different masses may be damped and one expects a small effect, $\lesssim 1$ ‰ , (Δm quark $\approx M_z$). More details are found in ref (20).

10.3.4 The Higgs mass dependence is weak. For 30, 60, 90 GeV one has ($M_z = 94$) [18].

δM_W(MeV)	M_H = 10 GeV	100 GeV	10 GeV
m_t = 30	70	0	- 160
m_t = 60	80	0	- 160
m_t = 90	70	0	- 160

for the shift δM_W if M_H deviates from 100 GeV (in this table we have taken δM_W=0 for M_H=100 GeV independantly of m_t). A 1 ‰ measurement thus may exclude a Higgs mass of ≈ 1 TeV.

10.3.5 Several Higgs fields[21]

Adding any number of Higgs doublets does not change the ρ-parameter ; their effects on M_W are in Δr. With two doublets one has[21],

m_z	m_1 (GeV)	m_2 (GeV)	m_p (GeV)	δM_W
M_z	100	10	10	80 MeV
$5\,M_z$	100	10	10	530 MeV
M_z	100	M_z	M_z	0

where m_z , m_1, m_2, m_p are the masses of the charged, scalars[18] and pseudoscalar spinless bosons. δM_W is the shift relative to the standard model with M_z = 94 and M_H = 100 GeV. More results are in ref (21). If the additional scalars are triplets, they enter into Δr (to our knowledge this has not been calculated, we are considering it) ; however their dominant effet is, at tree level already in $\rho \equiv M_z^2 c^2 / M_W^2 s^2$, if they have a vacuum expectation value.

10.3.6 Two-loop effects[22]

These have been recently considered for the case of a heavy degenerate fermion doublet. It turns out, that the small corrections (see 10.3.2) can only be overcome for very large masses (> few TeV), e.g. only for m_t > few TeV the shifts in M_W are measurable.

10.4 Conclusion

The asymmetry measurement on the Z^0 resonance are dominated by radiative corrections of the type

$$(\rho - \Delta r) + \text{subleading term}$$

If the correction is small (same as the subleading) it does not necessarily indicate small Δr as long as a cancellation occurs in $\delta\rho - \Delta r$. Such a cancellation would be dramatically exhibited with the help of a precision measurement of the W-mass !

11. CONCLUSION

Each of the four LEP experiments can measure in at least three ways the mass of the W boson at LEP 200 with an accuracy of the order of 100 MeV (or better). The integrated luminosity of 500 events/pb used in this study provides a better statistical accuracy (50-60 MeV) but it appears difficult to control the systematical uncertainties at such a level. All the methods proposed in this report which extends the work of (23) require the knowledge of the machine beam energy which gives in any case an absolute limit on the W mass measurement accuracy.

12. ACKNOWLEDGEMENTS

During the course of this work we have benefited from the help and suggestions of many colleagues. We would like to thank especially : G.BARBIELLINI, M. DAVIER, R. KLEISS, P. MATTIG.

Je remercie Mmes M. BONNAMY, O. CLAVELOU et O. MOUCHET pour la qualité de leur travail lors de la frappe, la mise en page et la présentation du texte et des figures.

In this table you will find some general properties of the detectors used in our simulation. It gives some mean detector behaviour but the simulation programs are a lot more detailed.

	Calorimetric measurement (L3)	Granular detector measurement (ALEPH - DELPHI - OPAL)
σ_E / E	E.M. Calorimeter $\frac{2.5\%}{\sqrt{E}} \oplus 6‰$	$\frac{12 - 20\%}{\sqrt{E}}$
	Had. Calorimeter $\frac{55\%}{\sqrt{E}} + 5\%$	$\frac{60\%}{\sqrt{E}}$, $\frac{100\%}{\sqrt{E}}$
	Muons $.4 \times 10^{-3}\, p$	$10^{-3}\, p$
Acceptances	$\lvert\cos\theta\rvert \leqslant .984$ for $\begin{cases} e,\gamma \\ \mu \\ h \end{cases}$	$\lvert\cos\theta\rvert \leqslant .98$ for e,γ,h calorimetry
	p_μ measured accurately over 70% of 4π	$\lvert\cos\theta\rvert \leqslant .965$ for charged track momentum measurement (DELPHI)
Typical Properties	Energy loss of hadrons in BGO 40±20% with $e/\pi = 1.4$	DELPHI :
	$E_{meas} = f_{BGO} E_{BGO} + E_{REST}$ ($f_{BGO} \sim 1.15$ M.C.)	. charged tracks measured in the central detector
		. γ : $E_\gamma > 500$ MeV ; lost if a hadron is "too close"
		. n,K^0_L : $E > 1$ GeV ; lost if a hadron is "too close"
		ALPEH : special algorithm to recover γ or neutral hadrons when a charged hadron is in the vicinity.

TABLE I

REFERENCES

(1) H. Keil - Report presented at this workshop.

(2) F.M. Renard "γγ/WW collisions and related processes at future colliders" Laboratoire de Physique Mathematique de Montpellier - PM:86-11 (April 1986) - and references therein.
G. Altarelli and A. Gabrielli - University of Rome, Preprint 1986.

(3) W. Alles, Ch. Boyer and A.J. Buras, Nucl. Phys. B119 (1977) 125.
F. Bletzacker and H.T. Nieh, Nucl. Phys. B124 (1977) 511.
R.W. Brown and K.O. Mikaelian, Phys. Rev. D19 (1979) 922.
U.J.F. Gaemers and G.J. Gounaris, Z. Phys. C1 (1979) 259.
J.F. Gunion and Z. Kunszt, Phys. Rev. D33 (1985) 665.
K. Hagiwara, R.D. Peccei, D. Zeppenfeld and K. Hikasa, DESY 86-058.

(4) K. Hagiwara, R.D. Peccei, D. Zeppenfeld and K. Hikasa, DESY 86-058.

(5) W. Wetzel in Physics at LEP - CERN 86-02 V1 p40.

(6) J. Bijnens, Z. Kunszt and D. Wyler - to be published -.

(7) E. Longo - Report presented at this workshop.

(8) G. Barbiellini et al., Physics at LEP - CERN 86-02 - V2 p1.

(9) A. Bilal, M. Davier, K. Hagiwara and P. Roudeau. W pair M.C. generator, private communication.

(10) M. Banner et al., LEP Summer Study, CERN 79-02 V2 p595.

(11) R.H. Schindler et al., Phys. Rev. D24 (1981) 78.
S. Behrends et al., Phys. Rev. Lett. 50 (1983) 881.
R. Giles et al., Phys. Rev. D30 (1984) 2279.

(12) H.U. Martyn - Precise W mass determination using the L3 calorimeters
Note ECFA LEP 200/004.

(13) T. Sjostrand - Computer Physics Communications 28 (1983) 229.

(14) P. Roudeau, Delphi note 85-49 phys 5 and Proceedings of the 13th International Winter Meeting on Fundamental physics - Cuenca - Spain 1985, p.210.

(15) P. Minkowski, Study presented in our working group.

(16) M. Consoli and A. Sirlin, Physics at LEP ed. J. Ellis and R. Peccei, CERN 86-02 V1 p63.
B.W. Lynnn, M. Peskin and R.G. Stuart, ibid p90.

(17) A. Sirlin, Phys. Rev. D22 (1980) 971.

(18) For a review and references see e.g. B. Lynn et al., in "Physics at LEP", CERN 86-02 V.1 ;
W. Hollik, DESY 86-049 (1986).

(19) See the first reference in (18) ; W. Marciano and A. Sirlin, BNL-33/819.

(20) B. Lynn, SLAC - PUB - 3358 (T/E).

(21) W. Hollik, DESY 86-047.

(22) J. Van der Bij and F. Hoogeveen, Fermilab - PUB 86/99T.

(23) G. Barbiellini, M. Davier, K. Hagiwara, R.D. Peccei, F. Schrempp, D. Zeppenfeld, H.U. Martyn, B. Schrempp and S. Yamada, DESY 86-018, see also "Physics at LEP" CERN 86-02, V2 p1.

(24) F. Jegerlehner, Zeit. Phys. C 32 (1986) 195.

(25) W. Marciano, Phys. Rev. D (1979).

FIGURE CAPTIONS

Fig.1 : W and Z production cross sections at LEP 200.

Fig.2 : Diagrams contributing to the radiative corrections in the process $e^+e^- \rightarrow W^+W^-$.

Fig.3 : Effect of radiative corrections on a reconstructed W mass distribution when the beam energy constraint is applied.

Fig.4 : Integrated cross-sections of the various processes occuring at LEP 200 (without radiative corrections).

Fig.5 : Hadronic production cross sections at LEP 200.

Fig.6 : Energy balance distributions in case of W pair events and other hadronic events.

Fig.7 : Energy balance distribution obtained when comparing the beam energy to the hadronic energy for events in which one W decays leptonically.

Fig.8 : W^+W^- production cross-section.

Fig.9 : a) Sensitivity of the W pair production cross section to W mass variations.
b) Error on M_W from 5 data points using various scenarii.

Fig.10 : Error on the W mass from 5 data points at 75, E-1, E, E+1 and 95 GeV as a function of E :
a) Background in the fit parametrized as b/s.
b) Background in the fit parametrized as a + b/s.
The curves are described in the text.

Fig.11 : Reconstructed energy distribution in granular detectors at E_{cm}= 60 GeV (2 jets events). We have compared two simulation programs realised for two different LEP experiments.

Fig.12 : Mean reconstructed energy and energy resolution for various c.m. energies.

Fig.13 : Reconstructed hadronic W mass distribution before and after "mass re-scaling" using a calorimetric approach.

Fig.14 : Reconstructed hadronic W mass distribution before and after "mass rescaling" using a granular detector.

Fig.15 : Expected mass distributions from background events. The content of these histograms has to be multiplied by 5 to correspond to a sensitivity of 500 events/pb. Fig.15-a assumes a top mass greater than M_W whereas in Fig.15-b M_t=35 GeV is used. Events entering into these distributions have to satisfy the cuts described in the text.

Fig.16 : Reconstructed W mass distributions when the W decays into hadrons.
a) One W decays leptonically, calorimetric approach.
b) Same conditions, granular detector approach (we have added in the histogram the $W \rightarrow \ell\nu$ reconstructed events and imposed a cut on energy balance at 10 GeV, see text).
c) The two W's decay into hadrons.

Fig. 17 : Reconstructed W mass distributions for leptonic decays.
a) We impose that the energy of the other W is equal to the beam energy.
b) We demand that the ν energy is equal to the difference between the beam and lepton energies.

Fig. 18 : Reconstructed Z^0 mass distribution in $e^+e^- \rightarrow \gamma Z^0$ events.
a) All events with $E_\gamma > 50$ GeV and $\theta_\gamma > 10°$.
b) Energy balance cut at 10 GeV.

Fig. 19 : Electron energy spectrum at $E_b = 95$ GeV.

Fig. 20 : Comparison of the electron energy distribution with predictions for $M_W = 81$, 82 and 83 GeV.

Fig. 21 : Variation of the reconstructed W width with the intrinsic width.

Fig. 22 : Expected accuracies on ρ and Δr from various experiments

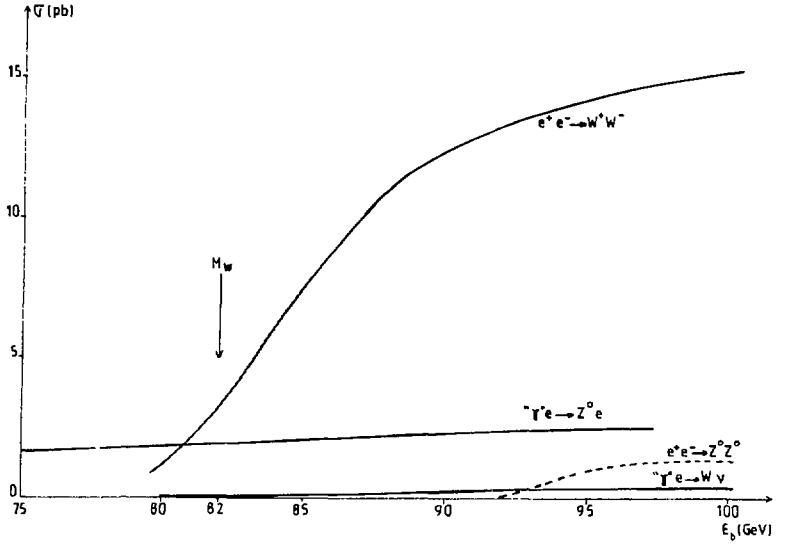

Fig. 1 : W and Z production cross sections

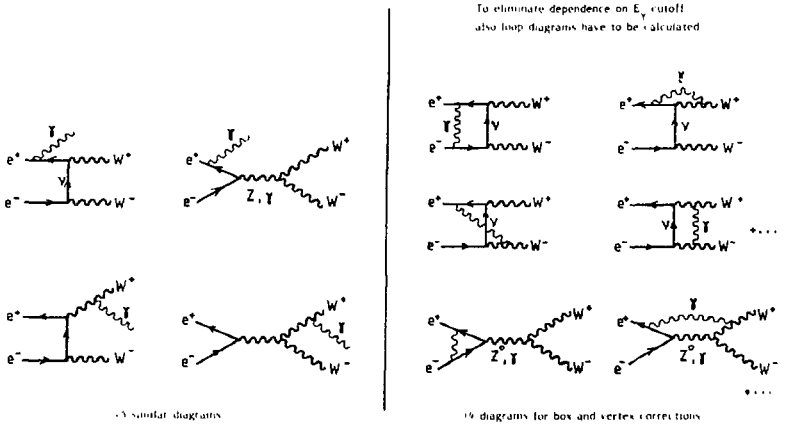

Fig. 2 : Diagrams contributing to radiative corrections

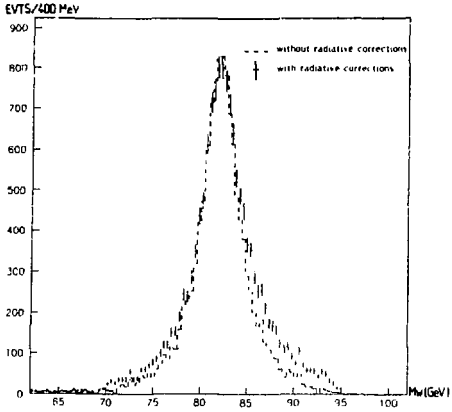

Fig. 3 : Effect of radiative corrections on a typical mass distribution after mass resuling

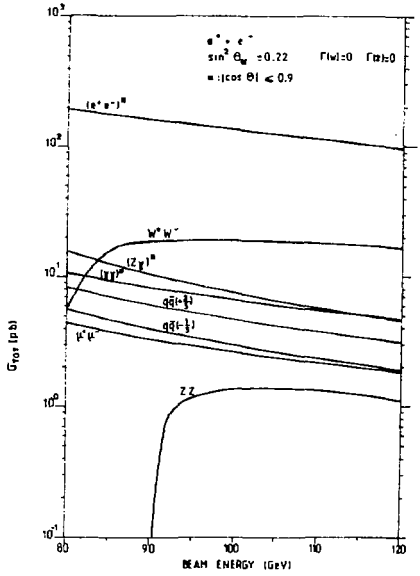

Fig. 4 : Integrated cross sections (without radiative corrections)

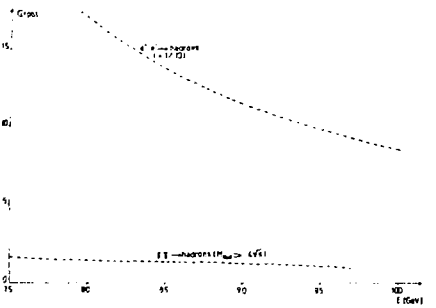

Fig. 5 : Hadronic cross sections

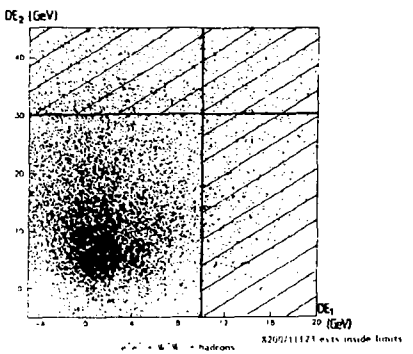

(× 1/4 for 500 evts/pb)

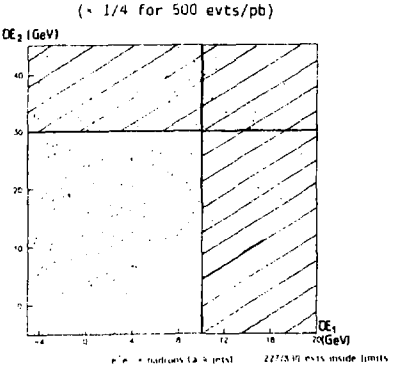

Fig. 6 : Background rejection in hadronic events

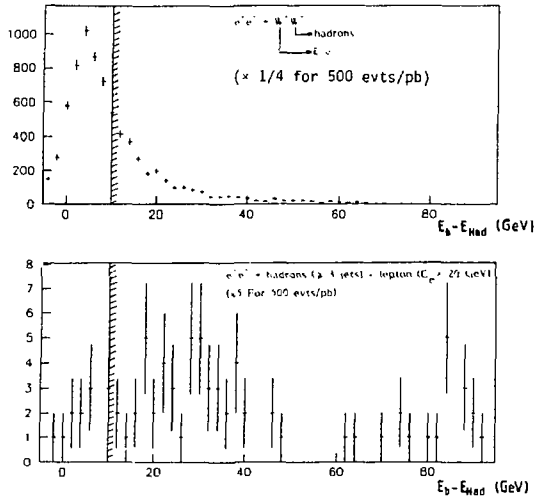

Fig.7 : Energy balance distribution between the beam and the hadronic system

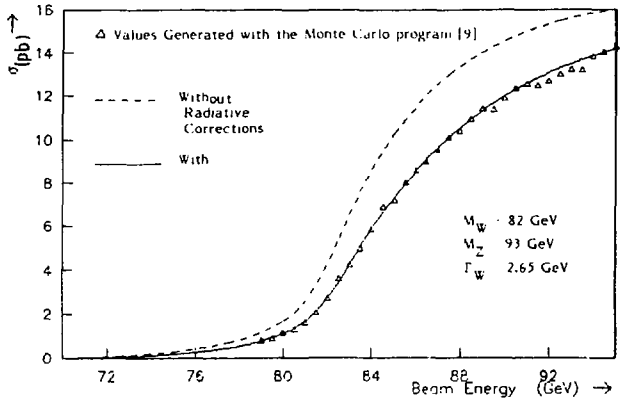

Fig.8 : Comparison of cross sections with and without radiative corrections

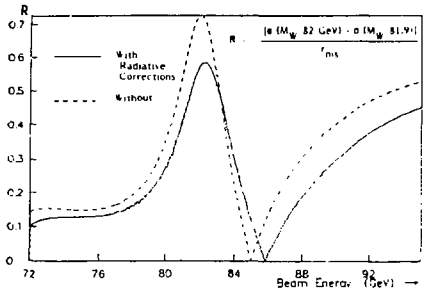

Fig. 9.a : Resolving power assuming 100 pb^{-1} at each beam energy

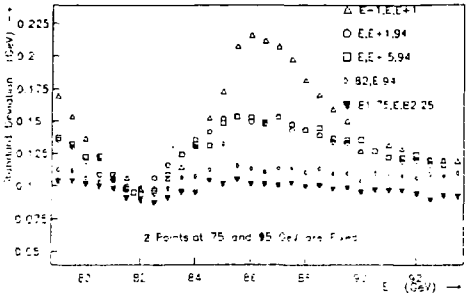

Fig. 9.b : Accuracy on the W mass

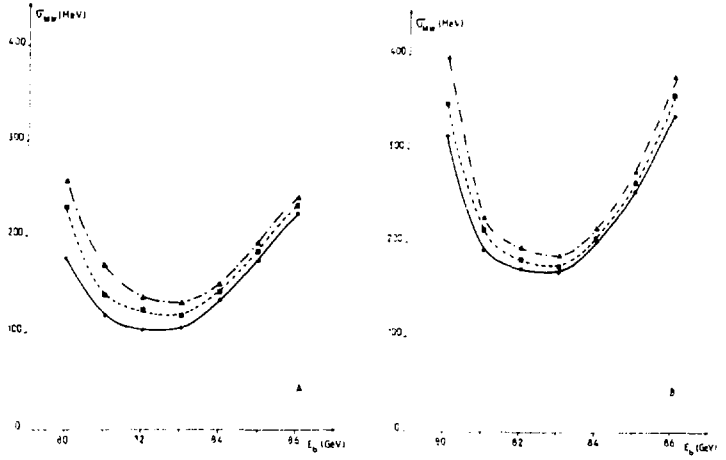

Fig. 10 W mass measurement accuracy from the threshold behaviour of the cross section in the presence of background

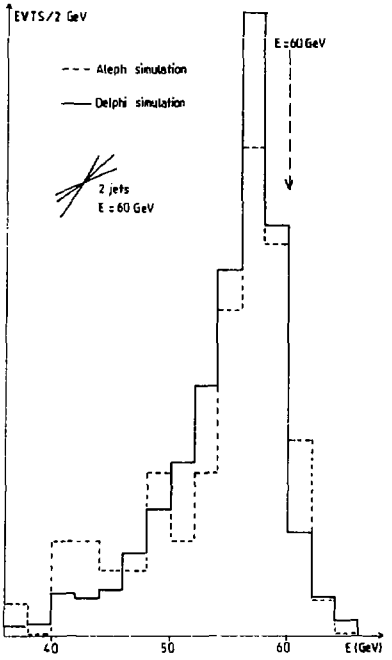

Fig. 11 : Distribution of the measured energy in "granular" detectors

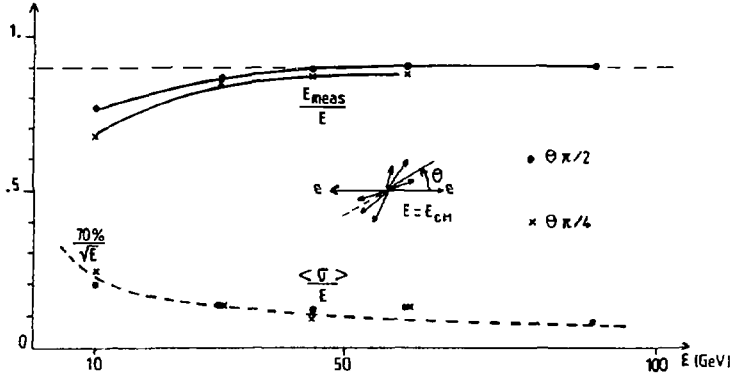

Fig. 12 : Energy reconstruction (ALEPH simulation)

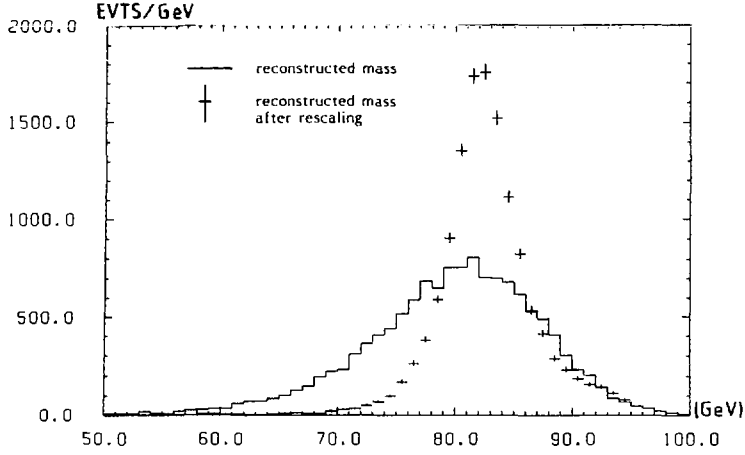

Fig.13 : Reconstructed mass distributions for class 1 events (calorimetric approach)

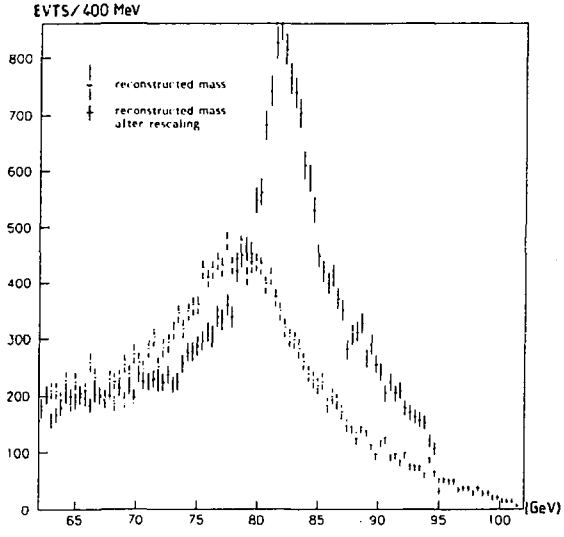

Fig.14 : Reconstructed mass distributions for class 2 events (granular detector approach)

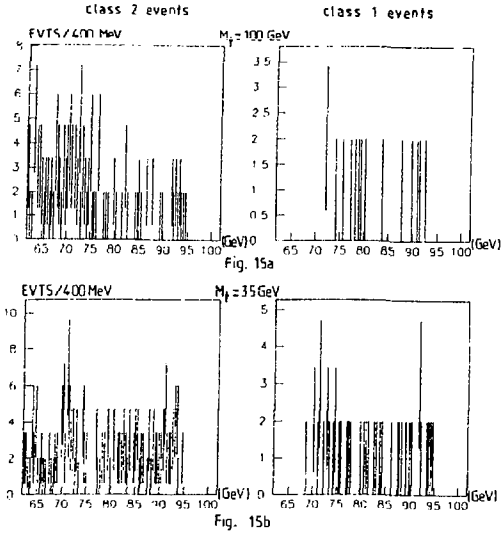

Fig. 15a

Fig. 15b

Fig. 15 : Mass distribution of background events. (x 5 for 500 evts/pb)

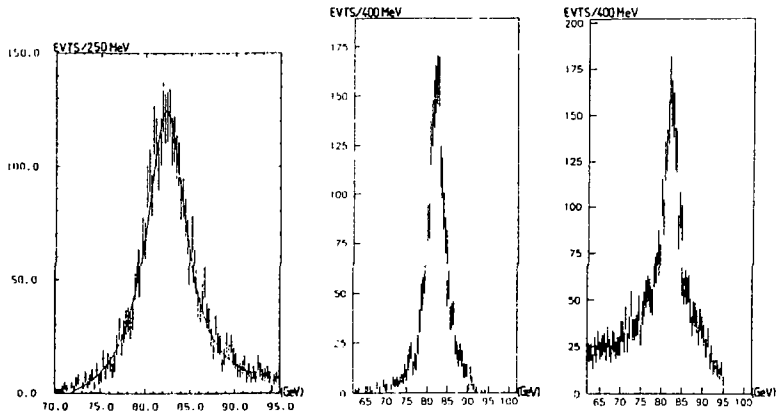

a) Class 1 events (calorimeter approach)

b) Class 1 events (granular detector approach)

c) Class 2 events (granular detector appraoch)

Fig. 16 : W mass reconstruction for W hadronic decays

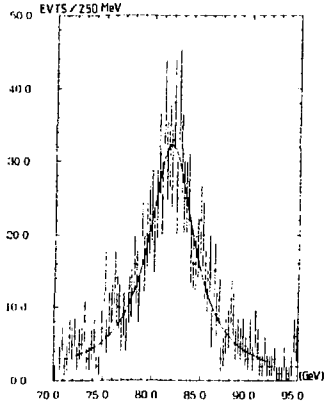

Fig. 17.a : $E_{had} = E_b$

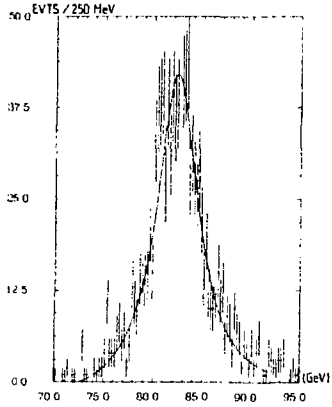

Fig. 17.b : $E_\nu = E_b - E_c$

Fig. 17 : $E-\nu$ mass distributions

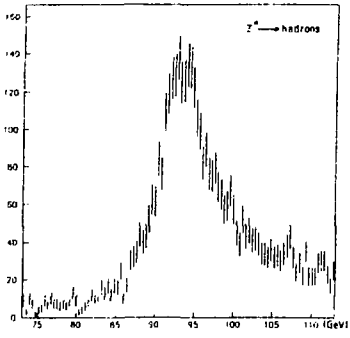

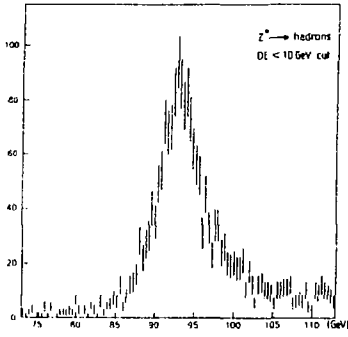

Fig. 18 : Reconstructed Z^0 mass distributions

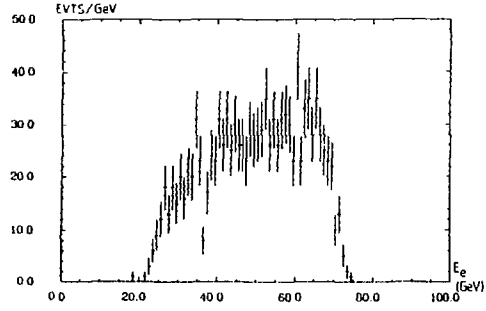

Fig. 19 : Electron energy distribution

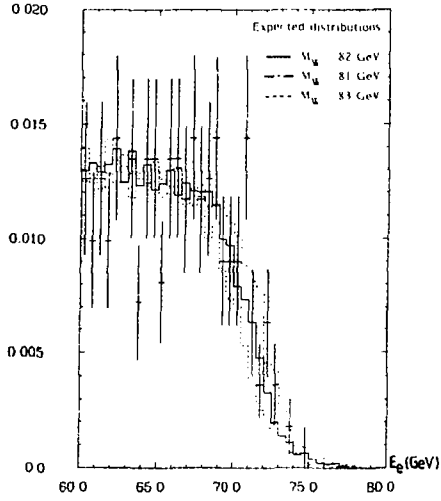

Fig. 20 : End-point of electron energy spectrum

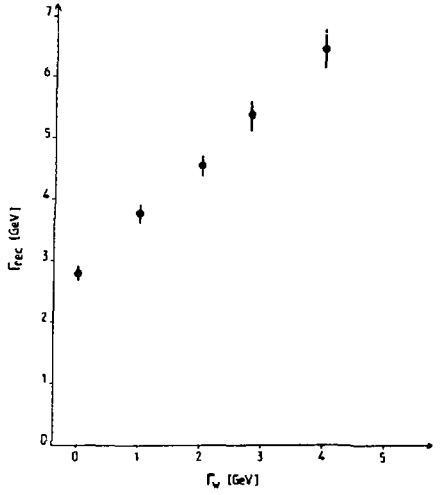

Fig. 21 : W width with measurement

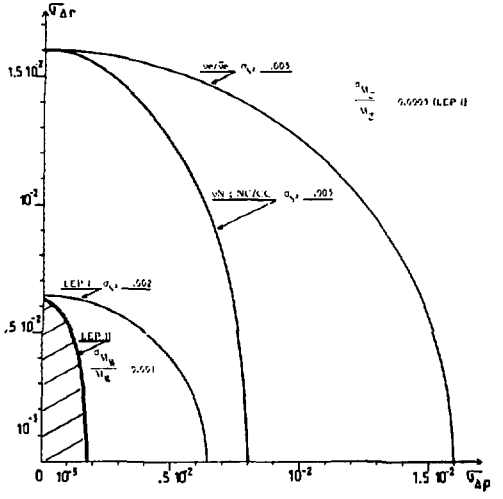

Fig. 22 : Expected accuracies on ρ and Δr from various experiments